Tokyo Climate Center, Japan Meteorological Agency

TCC News

Autumn 2022

Table of Contents: TCC News No. 70

El Niño Outlook (November 2022 - May 2023)

Atmospheric and oceanic indicators suggest ongoing La Niña conditions in the equatorial Pacific. It is likely that La Niña conditions will continue (80%) until boreal mid-winter and transfer to ENSO-neutral conditions by boreal spring (70%) (article based on the El Niño outlook issued on 10 November 2022).

1. El Niño/La Niña

In October 2022, the sea surface temperature (SST) for the NINO.3 region was below normal with a deviation of -0.9°C. SSTs were above normal in the western part and below normal in the central and eastern parts of the equatorial Pacific (Figures 1-1 and 1-3 (a)). Subsurface temperatures were above normal in the western part and below normal in the central and eastern parts (Figures 1-2 and 1-3 (b)). Atmospheric convective activity near the date line over the equatorial Pacific was below normal, and easterly winds in the lower troposphere (i.e., trade winds) over the central equatorial Pacific were stronger than normal. These oceanic and atmospheric conditions are consistent with characteristics commonly seen in past La Niña events during the maturity stage, and indicate that La Niña conditions remain ongoing in the area.

JMA's seasonal ensemble prediction system suggests that trade winds over the central equatorial Pacific will continue to be stronger than normal until early boreal winter due to atmosphere-ocean interaction. Related interaction will keep the NINO.3 index below -0.5°C until boreal mid-winter (Figure 1-4). In association with eastward migration of warm subsurface water in the western equatorial Pacific, the NINO.3 index will start to rise and approach normal in boreal spring. In conclusion, it is likely that La Niña conditions will continue (80%) until boreal mid-winter and transfer to ENSO-neutral conditions by boreal spring (70%) (Figure 1-5).

2. Western Pacific and Indian Ocean

The area-averaged SST in the tropical western Pacific (NINO.WEST) region was near normal in October. Index values are likely to be above or near normal until boreal spring.

The area-averaged SST in the tropical Indian Ocean (IOBW) region was below normal in October. Index values are likely to be below or near normal until boreal spring.

* The SST normal for the NINO.3 region (5°S – 5°N, 150°W – 90°W) is defined as a monthly average over the latest sliding 30-year period (1992-2021 for this year).

* The SST normals for the NINO.WEST region (Eq. – 15°N, 130°E – 150°E) and the IOBW region (20°S – 20°N, 40°E – 100°E) are defined as linear extrapolations with respect to the latest sliding 30-year period, in order to remove the effects of significant long-term warming trends observed in these regions.

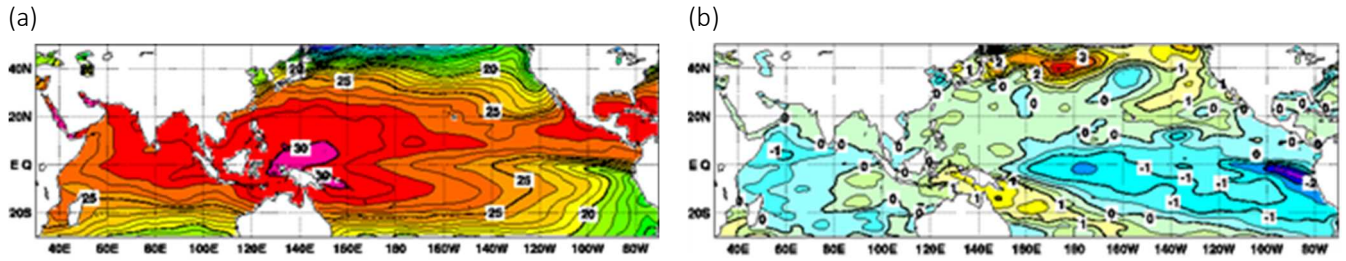

Figure 1-1 Monthly mean (a) sea surface temperatures (SSTs) and (b) SST anomalies in the Indian and Pacific Ocean areas for October 2022
The contour intervals are 1°C in (a) and 0.5°C in (b). The base period for the normal is 1991 – 2020.

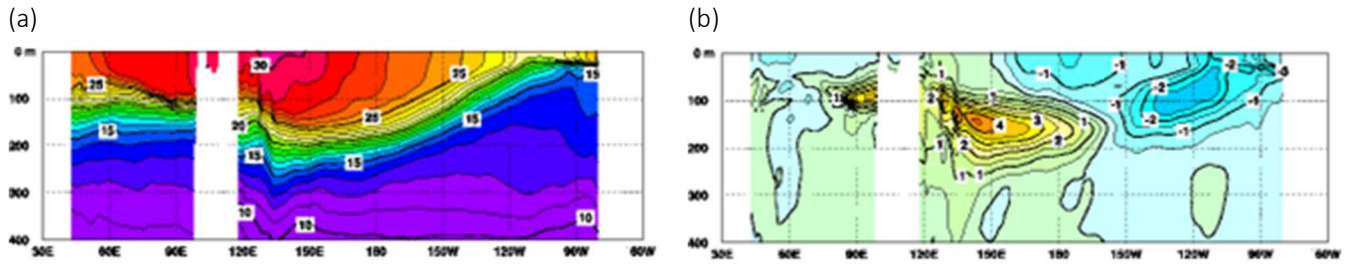

Figure 1-2 Monthly mean depth-longitude cross sections of (a) temperatures and (b) temperature anomalies in the equatorial Indian and Pacific Ocean areas for October 2022
The contour intervals are 1°C in (a) and 0.5°C in (b). The base period for the normal is 1991 – 2020.

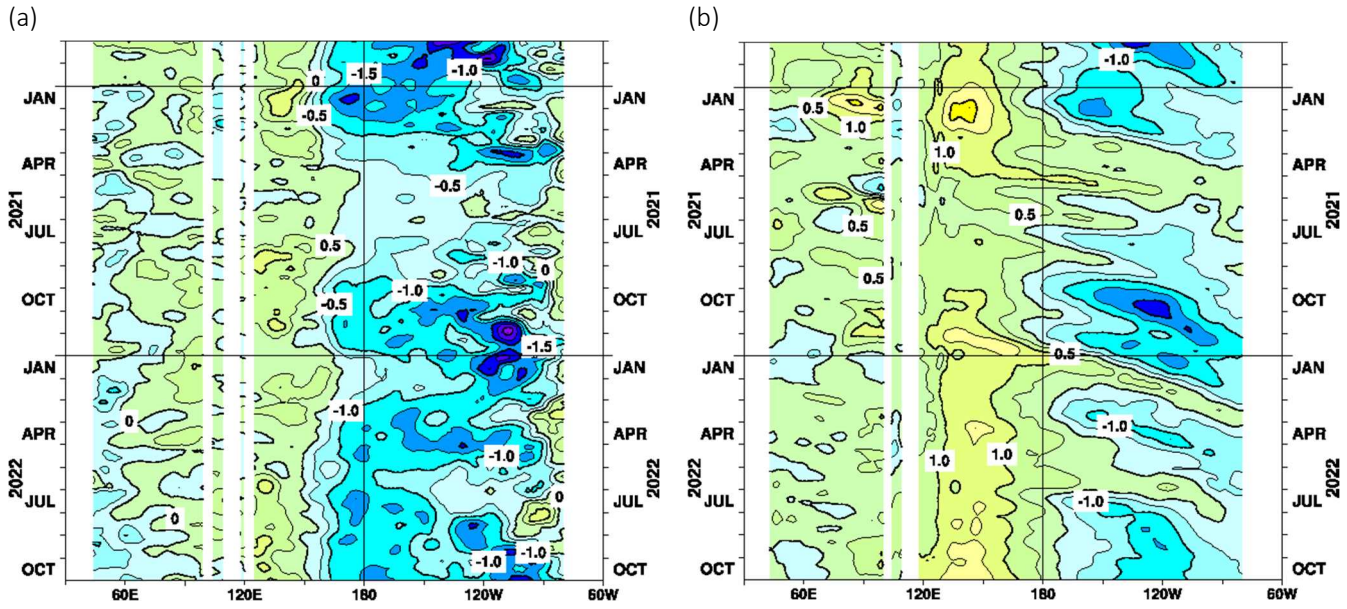

Figure 1-3 Time-longitude cross sections of (a) SST and (b) ocean heat content (OHC) anomalies along the equator in the Indian and Pacific Ocean areas

OHCs are defined here as vertically averaged temperatures in the top 300 m. The base period for the normal is 1991 – 2020.

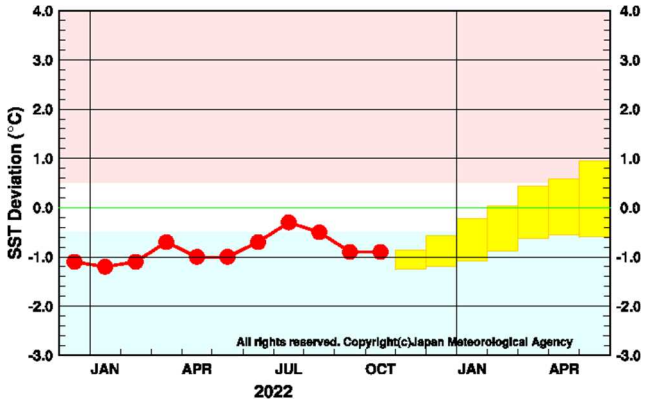

Figure 1-4 Outlook of NINO.3 SST deviation produced by the seasonal ensemble prediction system

This figure shows a time series of monthly NINO.3 SST deviations. The thick line with closed circles shows observed SST deviations, and the boxes show the values produced for up to six months ahead by the seasonal ensemble prediction system. Each box denotes the range into which the SST deviation is expected to fall with a probability of 70%.

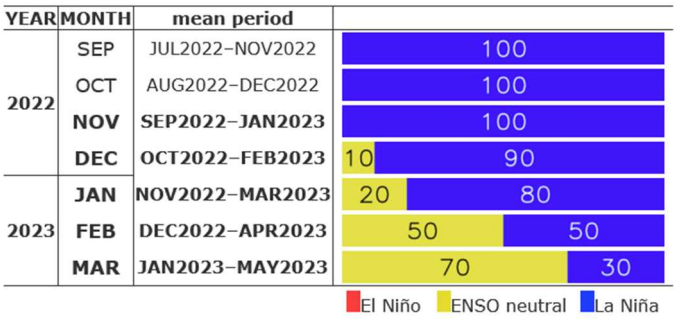

Figure 1-5 ENSO forecast probabilities based on the seasonal ensemble prediction system

Red, yellow and blue bars indicate probabilities that the five-month running mean of the NINO.3 SST deviation from the latest sliding 30-year mean will be +0.5°C or above (El Niño), between +0.4 and -0.4°C (ENSO-neutral) and -0.5°C or below (La Niña), respectively. Regular text indicates past months, and bold text indicates current and future months.

(SATO Hitoshi, Tokyo Climate Center)

<<Table of contents <Top of this article

JMA's Seasonal Numerical Ensemble Prediction for Boreal Winter 2022/2023

This report outlines JMA's dynamical seasonal ensemble prediction for boreal winter 2022/2023 (December – February, referred to as DJF), which was used as a basis for JMA's operational three-month outlook issued on 22 November 2022.

Summary: JMA's seasonal ensemble prediction system suggests that La Niña conditions are likely to continue until boreal mid-winter and transfer to ENSO-neutral conditions by boreal spring. In association with above-normal SSTs in the western tropical Pacific, enhanced convection is expected in and around Southeast Asia, resulting in upper-tropospheric anti-cyclonic circulation anomalies near southern China and a northward-meandering subtropical jet stream over the region.

1. Sea surface temperature

Figure 2-1 shows predicted SSTs (contours) and related anomalies (shading) for DJF. In the equatorial Pacific, negative anomalies in the central-to-eastern parts and positive anomalies in the western part are expected. La Niña conditions are likely to continue until boreal mid-winter and transfer to ENSO-neutral conditions by boreal spring. In the tropical Indian Ocean, negative anomalies are expected over a wide area.

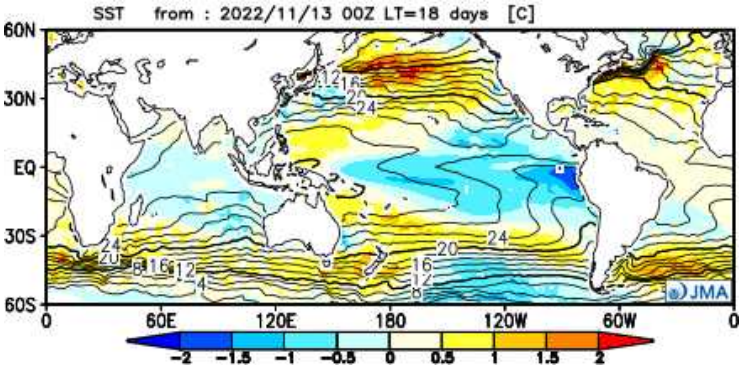

Figure 2-1 Predicted SSTs (contours) and SST anomalies (shading) for December–February 2022/2023 (ensemble mean of 51 members)

2. Prediction for the tropics and sub-tropics

Figure 2-2 (a) shows predicted precipitation (contours) and related anomalies (shading) for DJF. In association with the SST anomalies detailed above, above-normal precipitation is expected in and around Southeast Asia and below-normal precipitation is expected over the western-to-central equatorial Pacific and the southwestern tropical Indian Ocean.

Figure 2-2 (b) shows predicted velocity potential (contours) and related anomalies (shading) in the upper troposphere for DJF. Negative (i.e., large-scale divergent) anomalies are expected over Southeast Asia, while positive (i.e., large-scale convergent) anomalies are expected near the date line in the equatorial Pacific and over the southwestern tropical Indian Ocean.

Figure 2-2 (c) shows predicted stream functions (contours) and related anomalies (shading) in the upper troposphere for DJF. Anti-cyclonic (i.e., positive) circulation anomalies are expected near southern China, and cyclonic

(i.e., negative in the Northern Hemisphere) circulation anomalies straddling the equator are expected over the central tropical Pacific.

Figure 2-2 (d) shows predicted stream functions (contours) and related anomalies (shading) in the lower troposphere for DJF. Cyclonic (i.e., negative in the Northern Hemisphere) circulation anomalies straddling the equator are expected from the eastern tropical Indian Ocean to the Maritime Continent, and anti-cyclonic (i.e., positive in the Northern Hemisphere) circulation anomalies straddling the equator are expected near the date line over the equatorial Pacific.

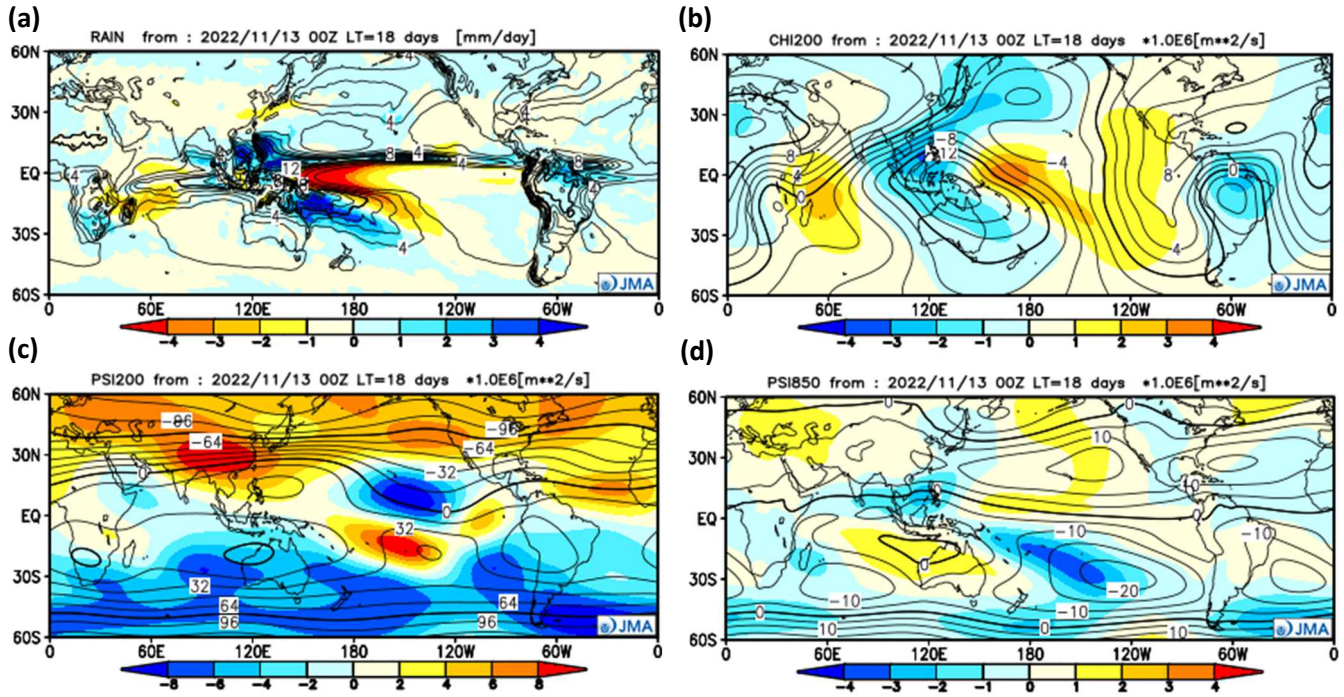

Figure 2-2 Predicted atmospheric fields over 60°N-60°S for December-February 2022/2023 (ensemble mean of 51 members)
(a) Precipitation (contours) and anomaly (shading). The contour interval is 2 mm/day. (b) Velocity potential at 200-hPa (contours) and anomaly (shading). The contour interval is 2×10^6 m^2/s. (c) Stream function at 200-hPa (contours) and anomaly (shading). The contour interval is 16×10^6 m^2/s. (d) Stream function at 850-hPa (contours) and anomaly (shading). The contour interval is 5×10^6 m^2/s.

3. Prediction for the mid- and high- latitudes of the Northern Hemisphere

Figure 2-3 (a) shows predicted 500-hPa geopotential heights (contours) and related anomalies (shading) for DJF. A wave train is expected from East Asia to North America, with negative anomalies over Japan and positive anomalies near the Aleutian Islands.

Figure 2-3 (b) shows predicted sea level pressure (contours) and related anomalies (shading) for DJF. In association with 500-hPa geopotential height anomalies, the Aleutian Low is expected to shift westward of its normal position and negative sea level pressure anomalies are expected over the northeastern part of East Asia.

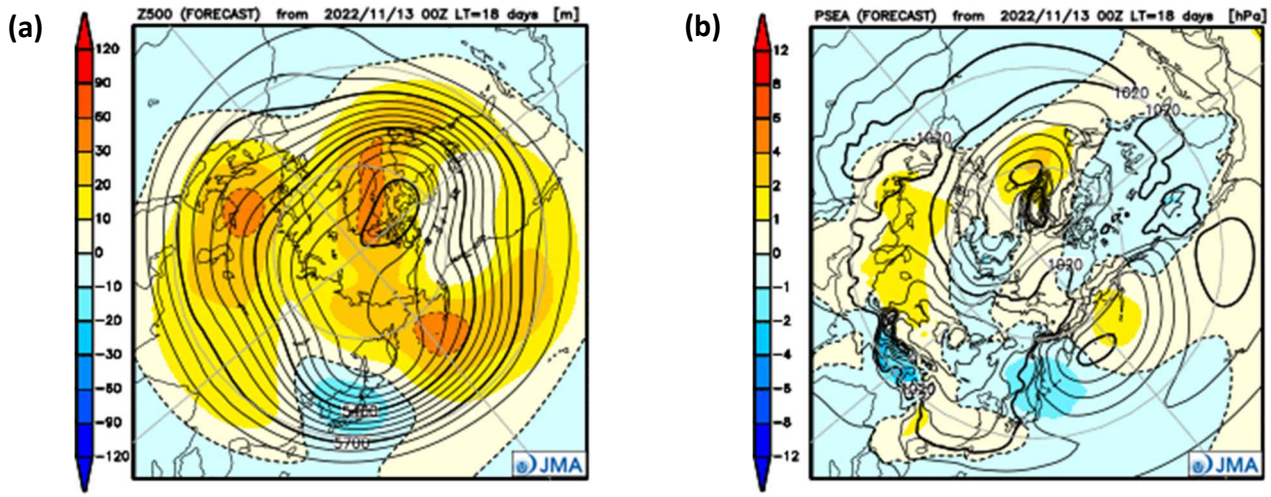

Figure 2-3 Predicted atmospheric fields in the Northern Hemisphere for December-February 2022/2023 (ensemble mean of 51 members)

(a) Geopotential height at 500-hPa (contours) and anomaly (shading). The contour interval is 60 m. (b) Sea level pressure (contours) and anomaly (shading). The contour interval is 4 hPa.

Note: JMA operates a seasonal Ensemble Prediction System (EPS) using the Coupled atmosphere-ocean General Circulation Model (CGCM) to make seasonal predictions beyond a one-month time range. The EPS produces perturbed initial conditions by means of a combination of the initial perturbation method and the lagged average forecasting (LAF) method. Prediction is made using 51 members from the latest 17 initial dates (3 members are used every day). Details of the prediction system and verification maps based on 30-year hindcast experiments (1991–2020) are available at https://www.data.jma.go.jp/tcc/tcc/products/model/.

(SATO Hitoshi, Tokyo Climate Center)

<<Table of contents <Top of this article

Summary of the 2022 Asian Summer Monsoon

This report summarizes the characteristics of the surface climate and atmospheric/oceanographic considerations related to the Asian summer monsoon for 2022.

Note: The Japanese 55-year Reanalysis dataset (JRA-55; Kobayashi et al. 2015) and COBE-SST (Ishii et al. 2005) were used to analyze atmospheric circulation and sea surface temperature (SST). NOAA Interpolated Outgoing Longwave Radiation (OLR) data (Liebmann and Smith 1996) from the U.S. NOAA Physical Sciences Laboratory (PSL) (https://psl.noaa.gov/data/gridded/data.interp_OLR.html) were used to infer tropical convective activity. The base period for the normal is 1991 to 2020. The term "anomaly" as used in this report refers to deviation from the normal.

1. Precipitation and temperature

CLIMAT data on four-month total precipitation for the summer monsoon season (June – September) show more than 140% of the normal in Pakistan, near northeastern China, in northern Japan and in southern Indonesia, while values less than 60% of the normal are seen from Central Asia to Mongolia and over parts of southern China (Figure 3-1 (a)). In particular, four-month total precipitation exceeding 200% of the normal was seen in and around Pakistan, and it was reported that heavy rain from June to August caused at least 2,130 fatalities from South Asia to Iran (sources: governments of Pakistan, India and Nepal, European Commission). Monthly precipitation in China was the second lowest on record for July and the third lowest for September since 1961 (China Meteorological Administration).

Four-month mean temperatures for the same period were above normal in many parts of the area from Central to East Asia, while values were below normal in and around Pakistan (Figure 3-1 (b)). It was reported that heatwaves caused 76 fatalities in Japan (Fire and Disaster Management Agency of Japan, as of 15 September). The monthly mean temperature in China was the highest on record for June and August since 1961 (China Meteorological Administration), and that in Hong Kong was the highest for July since 1884 (Hong Kong Observatory).

(a) (b)

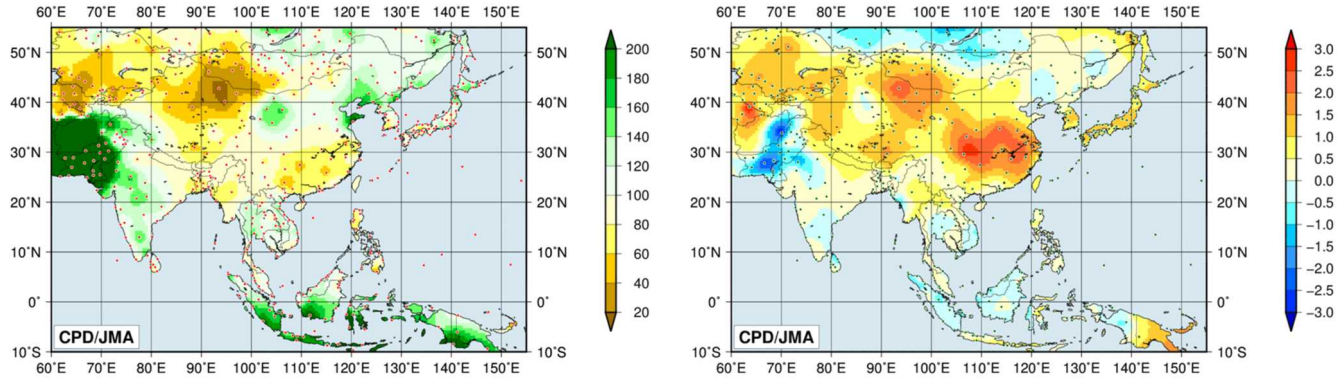

Figure 3-1 Four-month (a) precipitation ratios [%] and (b) mean temperature anomalies [°C] from June to September 2022

The base period for normal is 1991 – 2020. The red (a) and green (b) dots show stations providing map data, which are interpolated due to a lack of CLIMAT reporting and climatological normal values in some areas.

2. Tropical cyclones

A total of 18 named tropical cyclones (TCs) had formed over the western North Pacific and the South China Sea by the end of September 2022, as compared to the normal of 18.6 (Table 3-1). From June to September, a total of 16 named TCs (climatological normal: 16.1) formed, with 14 approaching or making landfall on Southeast and East Asia and 10 (climatological normal: 9.5) approaching or making landfall on Japan. A series of TCs formed over the latitude band of 20°N in the western North Pacific from August to September in association with the potential influences described in Section 3.

Table 3-1 Named Tropical cyclones which formed over the western North Pacific and the South China Sea by the end of September 2022

Name (number)		Date(UTC)	Category[1)]	Maximum wind[2)] (kt)
Malakas	(2201)	8 Apr - 15 Apr	TY	90
Megi	(2202)	9 Apr - 10 Apr	TS	40
Chaba	(2203)	30 Jun - 3 Jul	TY	70
Aere	(2204)	1 Jul - 4 Jul	TS	45
Songda	(2205)	28 Jul - 31 Jul	TS	40
Trases	(2206)	31 Jul - 1 Aug	TS	35
Mulan	(2207)	9 Aug - 10 Aug	TS	35
Meari	(2208)	11 Aug - 14 Aug	TS	40
Ma-On	(2209)	22 Aug - 25 Aug	STS	60
Tokage	(2210)	22 Aug - 25 Aug	TY	75
Hinnamnor	(2211)	28 Aug - 6 Sep	TY	105
Muifa	(2212)	8 Sep - 15 Sep	TY	85
Merbok	(2213)	12 Sep - 15 Sep	TY	70
Nanmadol	(2214)	13 Sep - 19 Sep	TY	105
Talas	(2215)	23 Sep	TS	35
Noru	(2216)	23 Sep - 28 Sep	TY	95
Kulap	(2217)	26 Sep - 29 Sep	STS	60
Roke	(2218)	28 Sep - 1 Oct	TY	70

Note: Based on information from the RSMC Tokyo-Typhoon Center.
1) Intensity classification for tropical cyclones.
TS: tropical storm (34 – 47 kt), STS: severe tropical storm (48 – 63 kt), TY: typhoon (≥64 kt)
2) Estimated maximum 10-minute mean wind.
3) Based on early analysis data (rather than best track data) for tropical cyclones from Meari (2208) to Roke (2218).

3. Monsoon activity and atmospheric circulation

Convective activity inferred from OLR averaged for June – September 2022 (Figure 3-2) was enhanced from the southeastern tropical Indian Ocean to Indonesia, from the Arabian Peninsula to western India through Pakistan, and over the latitude band of 20°N in the western North Pacific, while convective activity was suppressed from the Indochina Peninsula to the seas east of the Philippines and in the western equatorial Pacific. The anomalous convection observed from the southeastern tropical Indian Ocean to the western equatorial Pacific is associated with a negative Indian Ocean Dipole (IOD) mode, which is characterized by positive SST anomalies in the southeastern tropical Indian Ocean, negative SST anomalies in the western tropical Indian Ocean, and the La Niña event (Figure 3-3). OLR index data (Table 3-2) indicate that the overall activity of the Asian summer monsoon (represented by the SAMOI (A) index) was above normal in May and below normal from June to August. The active convection area was shifted southward of its normal position in May, July and August, and northward in June and September (see SAMOI (N) index).

Although the average activity of the Asian monsoon was weaker than normal during summer, convective activity in the Asian monsoon region exhibited remarkable intraseasonal oscillation. It was enhanced over India and the Bay of Bengal (Figure 3-4 (a)) in early July, early August and early September, suppressed in late July and late August, enhanced over the Philippines (Figure 3-4 (b)) in late June and early August, and suppressed in the first half of June, late July and late August. Such large fluctuations generally correspond to a large-amplitude boreal summer intraseasonal oscillation (BSISO; Lee et al. 2013; Kikuchi 2021).

Figure 3-5 shows four-month mean 200- and 850-hPa stream function fields for June – September. In the upper troposphere (Figure 3-5 (a)), anti-cyclonic circulation anomalies were seen along the latitude band of 40°N over Eurasia and the seas east of northern Japan, while cyclonic circulation anomalies were seen from South Asia to the northern tropical Indian Ocean, indicating a northward extension of the Tibetan high. Cyclonic circulation anomalies straddling the equator were also seen over the western tropical Pacific in association with La Niña-related suppressed convection in the western equatorial Pacific. In the lower troposphere (Figure 3-5 (b)), cyclonic circulation anomalies straddling the equator were seen over the eastern tropical Indian Ocean, while anti-cyclonic circulation anomalies straddling the equator were seen over the western tropical Pacific. The North Pacific Subtropical High extended southwestward of its climatological normal extent, and the monsoon trough over Southeast Asia was weaker than normal. These lower tropospheric circulation anomalies correspond to responses to anomalous tropical convection associated with the negative IOD and the La Niña event (Figures 3-2 and 3-3). The upper-level anti-cyclonic circulation anomalies observed to the east of northern Japan (Figure 3-5 (a)) are associated with lower-level anomalies over the area (Figure 3-5 (b)) with a near-equivalent barotropic structure.

Upper-level anticyclonic circulation anomalies to the east of northern Japan are presumed to play an important role in causing anomalous circulation over the subtropical western North Pacific. Figure 3-6 shows four-month mean isentropic potential vorticity (PV) at the 360 K surface for June – September. In association with upper-level anti-cyclonic circulation anomalies, clear low-PV anomalies were seen to the east of northern Japan. By contrast, high-PV anomalies were observed over a wide area in the subtropical western North Pacific. These upper-level anomalous PV characteristics imply frequent Rossby wave breaking (e.g., Postel and Hitchman 1999, 2001; Abatzoglou and Magnusdottir 2006) from Japan to the east, causing frequent southwestward intrusions of high-PV air masses toward the subtropical western North Pacific. Note that the equatorward-intruding high-PV air masses correspond to an upper-level cut-off cold vortex, promoting dynamically induced ascent over the area (e.g., Takemura et al. 2017),

enhanced convection over the latitude band of 20°N in the western North Pacific (Figure 3-2) and a series of TC formations from August to September (see Table 3-1, Section 2).

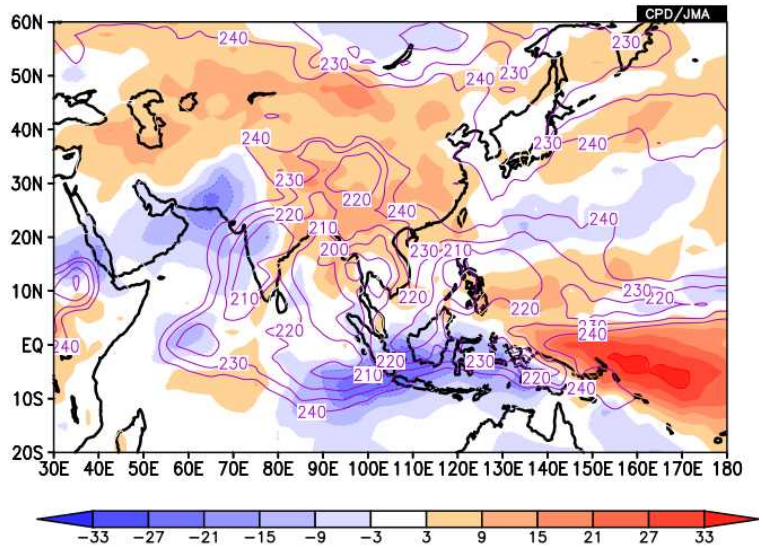

Figure 3-2 Four-month mean OLR [W/m^2] for June–September 2022

Contours indicate OLR lower than 240 W/m^2 at intervals of 10 W/m^2, and color shading denotes OLR anomalies from the normal (i.e., the 1991–2020 average). Negative (cold color) and positive (warm color) OLR anomalies show enhanced and suppressed convection compared to the normal, respectively.

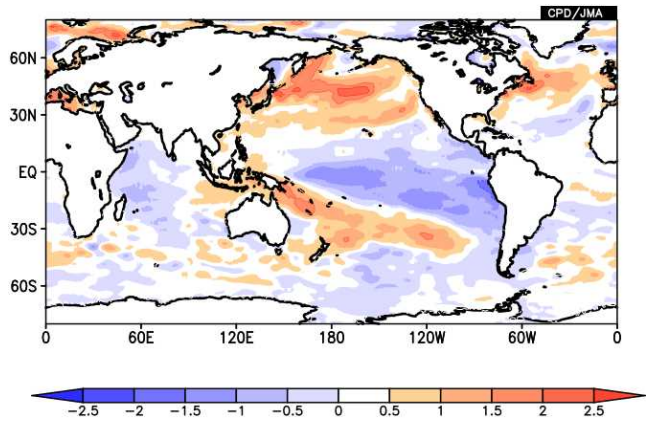

Figure 3-3 Four-month mean SST anomalies [°C] for June–September 2022

The base period for the normal is 1991 – 2020.

Table 3-2 Summer Asian Monsoon OLR Index (SAMOI) values observed from May to September 2022

Asian summer monsoon OLR indices (SAMOI) are derived from OLR anomalies. SAMOI (A), (N) and (W) indicate the overall activity of the Asian summer monsoon, its northward shift and its westward shift, respectively. SAMOI definitions are as follows: SAMOI (A) = (-1) × (W + E); SAMOI (N) = S – N; SAMOI (W) = E – W. W, E, N and S indicate area-averaged OLR anomalies for the respective regions shown in the figure on the right normalized by their standard deviations.

	Summer Asian Monsoon OLR Index (SAMOI)		
	SAMOI (A): Activity	SAMOI (N): Northward-shift	SAMOI (W): Westward-shift
May 2022	+0.7	-0.9	+0.8
Jun 2022	-1.6	+0.8	+0.7
Jul 2022	-0.8	-1.2	-1.1
Aug 2022	-0.7	-0.9	-0.4
Sep 2022	-0.1	+0.8	-0.8

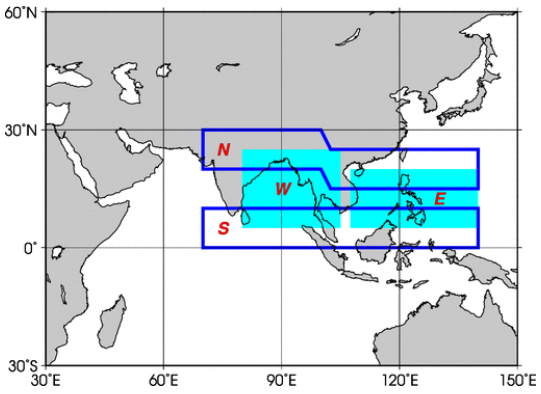

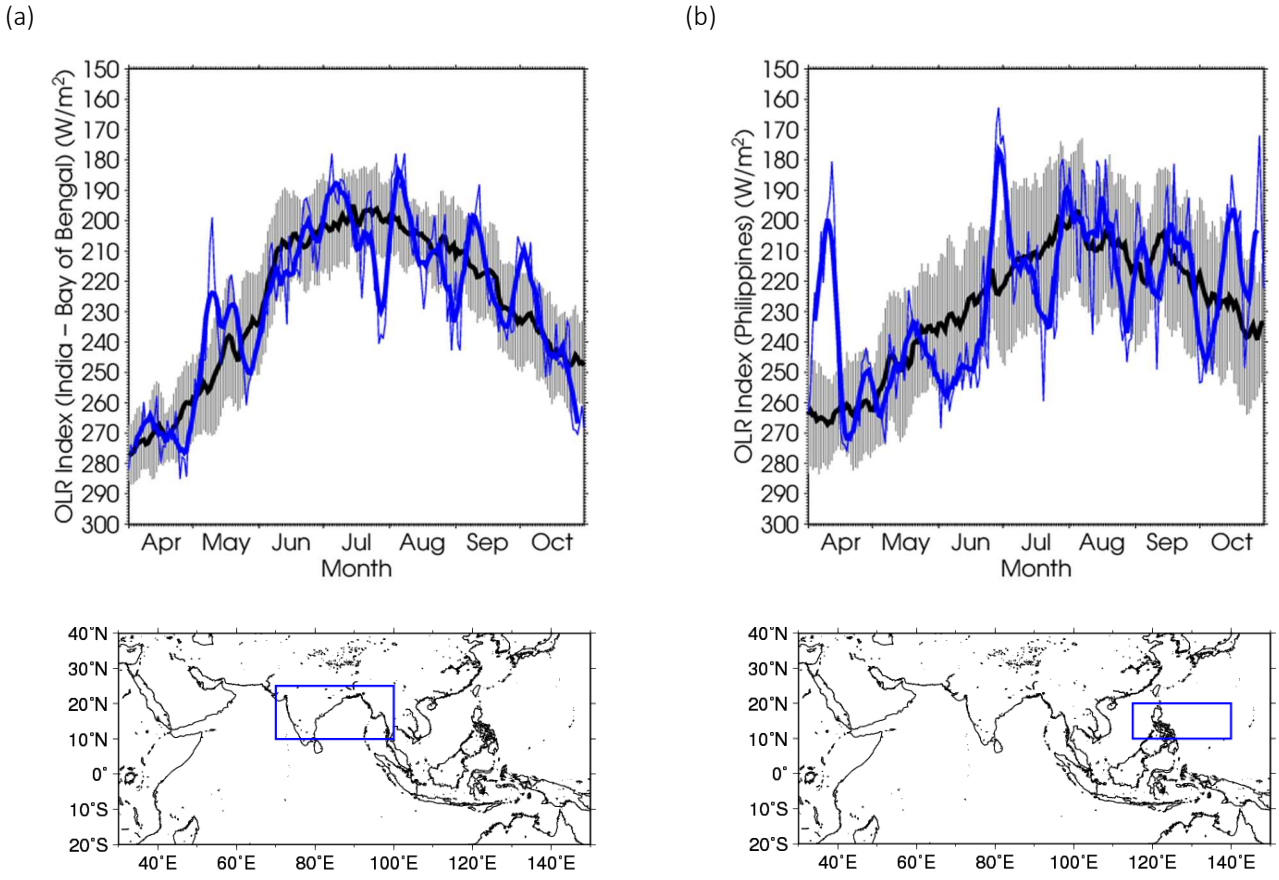

Figure 3-4 Time-series representation of OLR [W/m^2] averaged over (a) India and the Bay of Bengal (shown by the rectangle on the bottom: 10°N - 25°N, 70°E - 100°E) and (b) the Philippines (shown by the rectangle on the bottom: 10°N - 20°N, 115°E - 140°E)

The OLR indices are calculated after Wang and Fan (1999). The thick and thin blue lines indicate seven-day running mean and daily mean values, respectively. The black line denotes the normal (i.e., the 1991 - 2020 average), and the gray shading shows the range of the standard deviation calculated for the time period of the normal.

(a) (b)

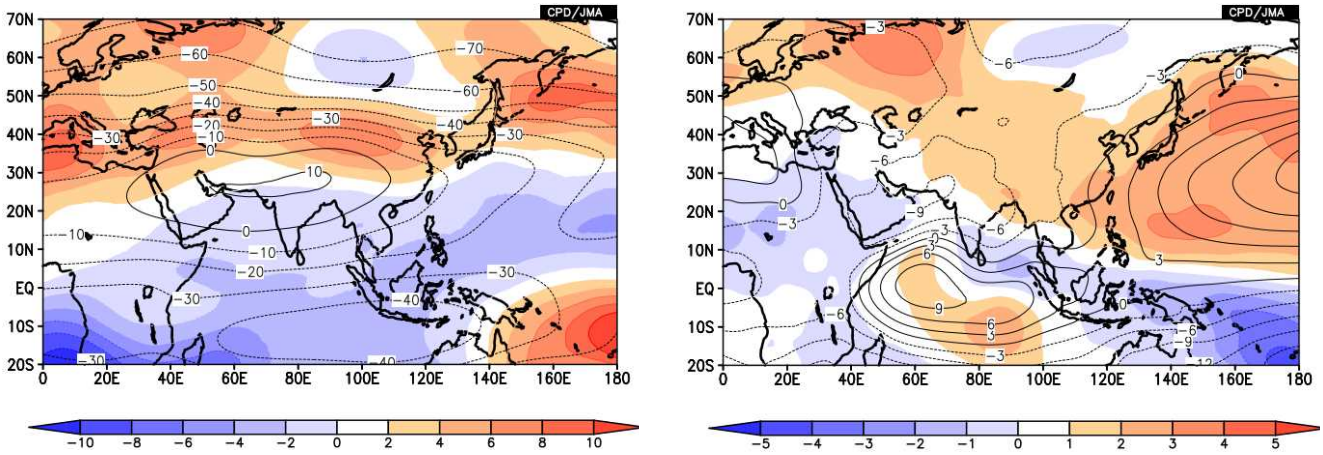

Figure 3-5 Four-month mean (a) 200-hPa and (b) 850-hPa stream function [10^6 m^2/s] for June–September 2022

Contours indicate stream function at intervals of (a) 10 × 10^6 m^2/s and (b) 3 × 10^6 m^2/s, and shading shows stream function anomalies. Red (blue) shading denotes anti-cyclonic (cyclonic) circulation anomalies in the Northern Hemisphere, and vice-versa in the Southern Hemisphere. The base period for the normal is 1991 – 2020.

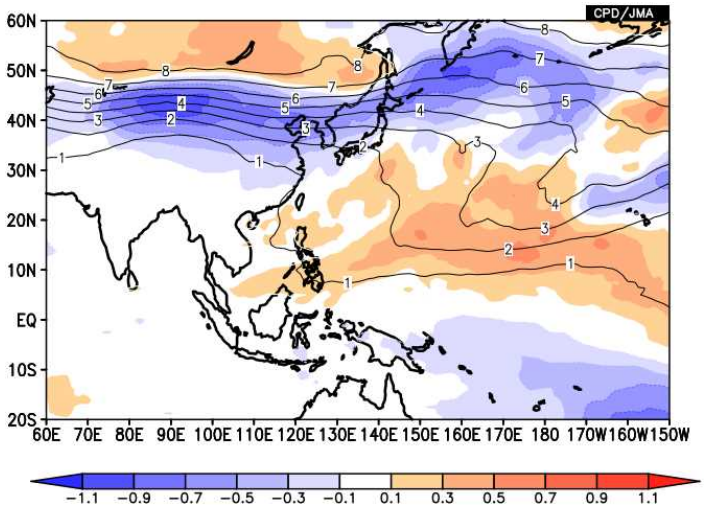

Figure 3-6 Four-month mean 360-K isentropic potential vorticity [PVU; $10^{-6}m^2s^{-1}K$ kg^{-1}] for June–September 2022

Shading indicates anomalies, and contours show potential vorticity at intervals of 1 PVU. The base period for the normal is 1991 – 2020.

References

Abatzoglou, J. T., and G. Magnusdottir, 2006: Planetary wave breaking and nonlinear reflection: Seasonal cycle and interannual variability. *J. Climate*, **19**, 6139-6152.

Ishii, M., A. Shouji, S. Sugimoto, and T. Matsumoto, 2005: Objective analyses of sea-surface temperature and marine meteorological variables for the 20th century using ICOADS and the Kobe Collection. *Int. J. Climatol.*, **25**, 865-879.

Kikuchi, K., 2021: The boreal summer intraseasonal oscillation (BSISO): A review. *J. Meteor. Soc. Japan*, **99**, 933-972.

Kobayashi, S., Y. Ota, Y. Harada, A. Ebita, M. Moriya, H. Onoda, K. Onogi, H. Kamahori, C. Kobayashi, H. Endo, K. Miyaoka, and K. Takahashi, 2015: The JRA-55 Reanalysis: General specifications and basic characteristics. *J. Meteor. Soc. Japan*, **93**, 5 – 48.

Lee, J.-Y., B. Wang, M. C. Wheeler, X. Fu, D. E. Waliser, and I.-S. Kang, 2013: Real-time multivariate indices for the boreal summer intraseasonal oscillation over the Asian summer monsoon region. *Clim. Dyn.*, **40**, 493-509.

Liebmann, B., and C. A. Smith, 1996: Description of a complete (interpolated) outgoing longwave radiation dataset. *Bull. Amer. Meteor. Soc.*, **77**, 1275-1277.

Postel, G. A., and M. H. Hitchman, 1999: A climatology of Rossby wave breaking along the subtropical tropopause. *J. Atmos. Sci.*, **56**, 359-373.

Postel, G. A., and M. H. Hitchman, 2001: A case study of Rossby wave breaking along the subtropical tropopause. *Mon. Wea. Rev.*, **129**, 2555-2569.

Takemura, K., Y. Kubo, and S. Maeda, 2017: Relation between a Rossby wave-breaking event and enhanced convective activities in August 2016. *SOLA*, **13**, 120-124.

Wang, B. and Z. Fan, 1999: Choice of South Asian summer monsoon indices. *Bull. Amer. Meteor. Soc.*, **80**, 629–638.

(Kazuto Takemura, Tokyo Climate Center)

<<Table of contents <Top of this article

Status of the Antarctic Ozone Hole in 2022

The size of the Antarctic ozone hole in 2022 exceeded the most recent decadal average due to a large low-temperature area in the stratosphere as in 2021.

Since the early 1980s, the Antarctic stratospheric ozone level has fallen every year in austral spring with a peak in September or early October. This area of depletion is referred to as the Antarctic ozone hole.

JMA analysis based on data from the Ozone Mapper Profiler Suite (OMPS) on board the Suomi National Polar-orbiting Partnership (NPP) satellite indicates that the 2022 Antarctic ozone hole had appeared by mid-August and expanded rapidly from late August onward, exceeding the scale of the most recent decadal average (Figure 4-1, upper left). Its annual maximum size (observed on 5 October) was 26.4 million square kilometers (Figure 4-1, upper right), which is slightly larger than that observed in 2021 and around 1.9 times as large as the Antarctic itself. In 2022 the polar vortex over Antarctica was large and dominant, and the low-temperature area in the stratosphere was larger than the most recent decadal average after late July. These conditions contributed to the year's expanded Antarctic ozone hole via increased formation of polar stratospheric clouds (PSCs), which play an important role in ozone depletion.

The *WMO/UNEP Scientific Assessment of Ozone Depletion: 2022* reports that total column ozone in the Antarctic continues to recover, notwithstanding substantial interannual variability in the size, strength and longevity of the ozone hole, and is expected to return to 1980 values around 2066.

The ozone layer acts as a shield against ultraviolet radiation, which can cause skin cancer. The Antarctic ozone hole was first recognized in the early 1980s, and large-scale events have been observed since the 1990s. Its record size was 29.8 million square kilometers (2000). Antarctic ozone depletion caused an expansion of the tropics and a poleward shift of the jet stream and storm tracks in the Southern Hemisphere that led to pronounced changes in summertime surface climate conditions according to recent assessment.

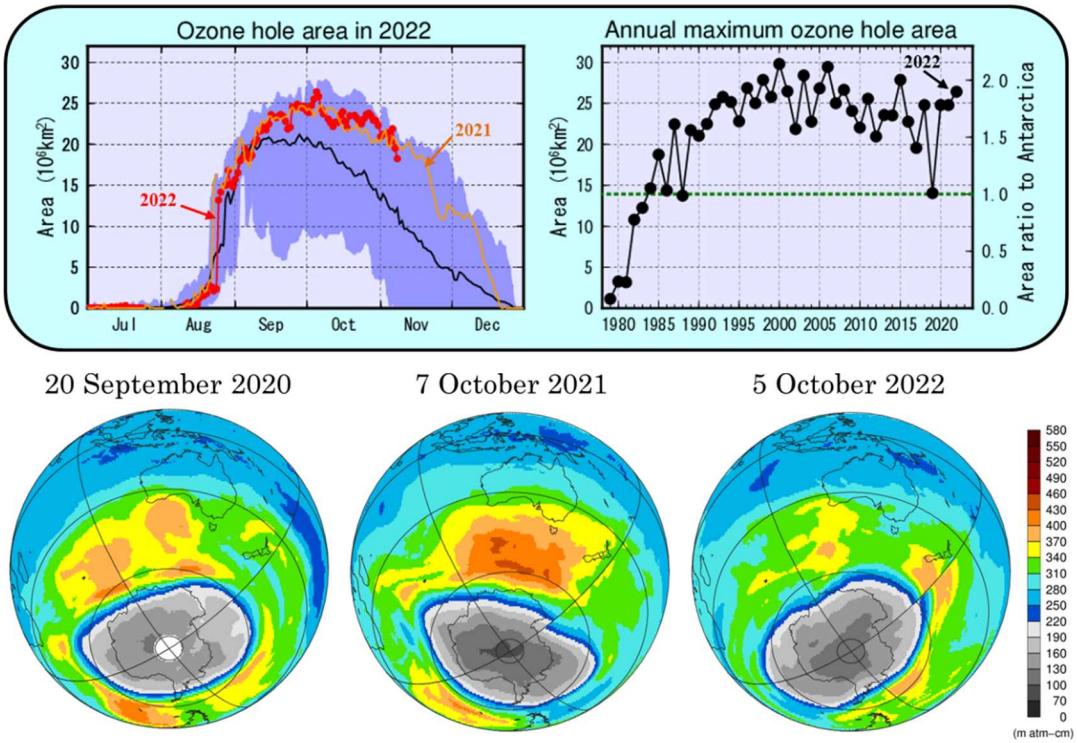

Figure 4-1 Antarctic ozone hole observation

Upper left: Time-series representation of the daily ozone hole area for 2022 (red line), 2021 (orange line) and the 2012 – 2021 average (black line). Blue shading represents the range of daily maxima and minima over the previous 10 years. JMA defines the extent of Antarctic ozone hole expansion area expanding as the area in which the total ozone column value is less than or equal to 220 m atm-cm.

Upper right: Inter-annual variability of the annual maximum ozone hole area. The green dotted line shows the area of the Antarctic Continent (13.9 million square kilometers).

Bottom: Snapshots of total column ozone distribution on the day of the annual maximum ozone hole area for the previous three years; the Antarctic ozone hole is shown in grey. Images are based on NASA satellite data.

(UEMURA Keiko, Atmospheric Environment and Ocean Division)

<<Table of contents <Top of this article

Status of the Arctic Sea Ice in 2022

It is virtually certain that there has been a long-term decreasing trend of sea ice extent in the Arctic Ocean since 1979, when the current method of monitoring using satellite sensors began. The trend is statistically significant at a confidence level of 99%. The reduction in the annual minimum extent is particularly notable at 0.087×10^6 km^2 per year up to 2022 (Figure 5-1).

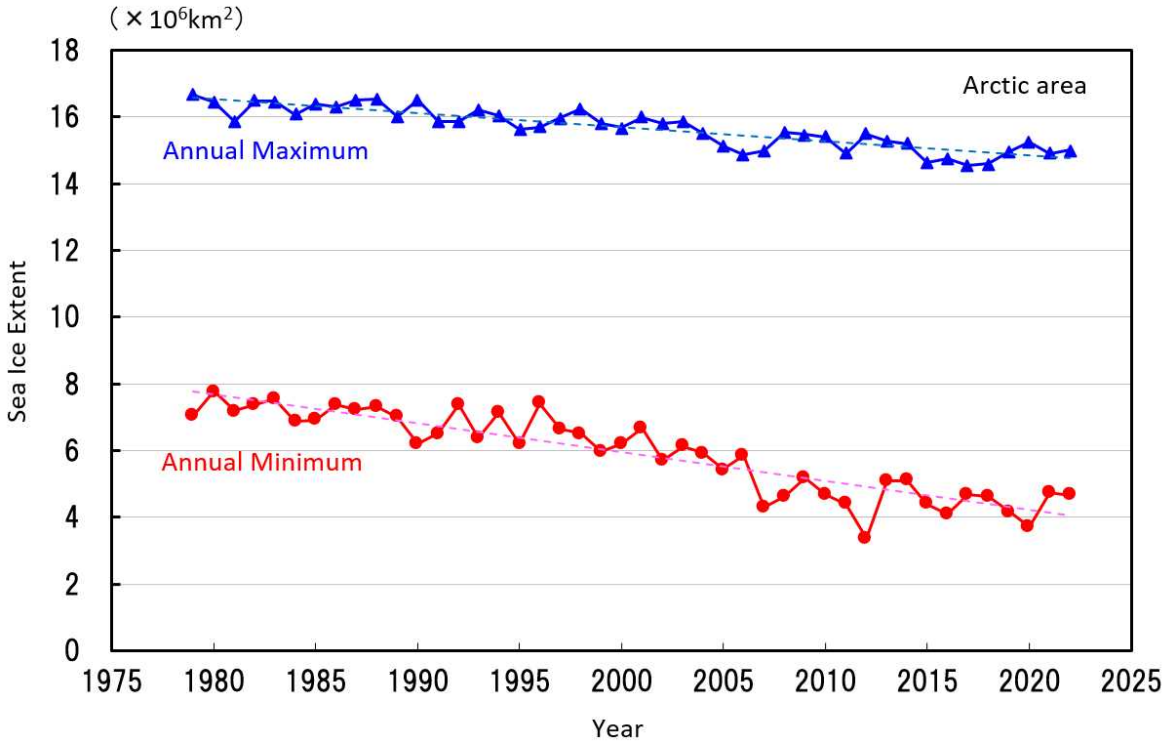

Figure 5-1 Time-series representations of annual maximum and annual minimum sea ice extent in the Arctic Ocean (including the Sea of Okhotsk and the Bering Sea) from 1979 to 2022

Blue and red lines indicate annual maximum and annual minimum sea ice extents, respectively, with dashed lines indicating linear trends. Sea ice extents are calculated from brightness temperature data provided by NASA (the National Aeronautics and Space Administration) and NSIDC (the National Snow and Ice Data Center).

Based on preliminary analysis, the annual maximum Arctic sea ice extent was 15.01×10^6 km^2 on 22 February 2022, marking the 10th-lowest value since 1979. The value subsequently decreased during spring and summer in the Northern Hemisphere and reached its annual minimum of 4.66×10^6 km^2 on 16 September, marking the 10th-lowest level since 1979 (Figure 5-2, 5-3).

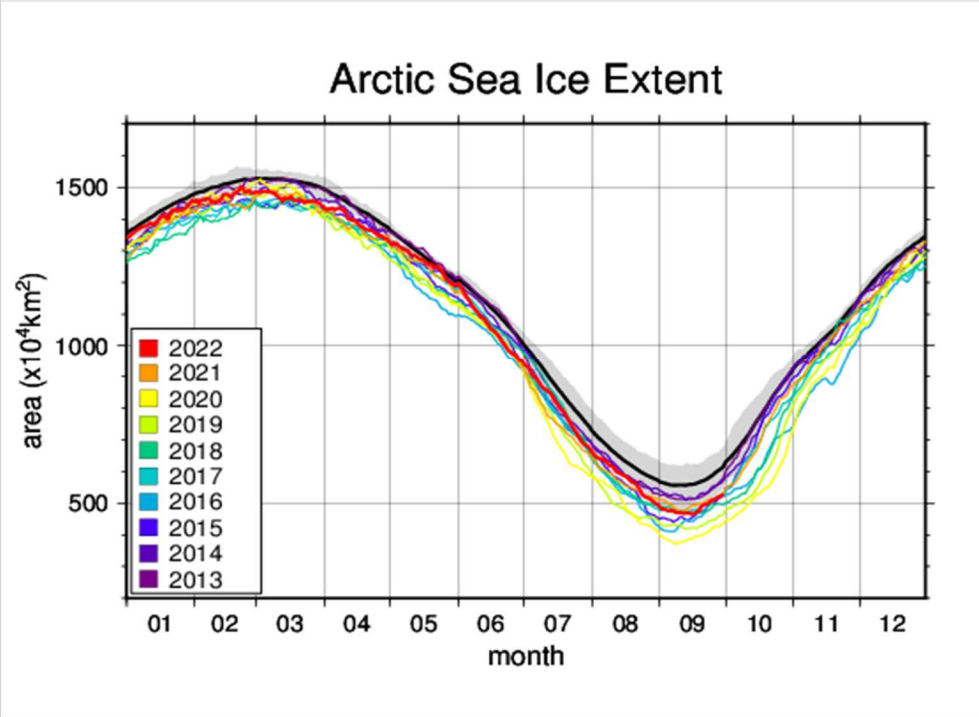

Figure 5-2 Annual variations in the Arctic sea ice extent
The black line represents the normal, and shading represents the normal range. The base period for the normal is 1991 – 2020.

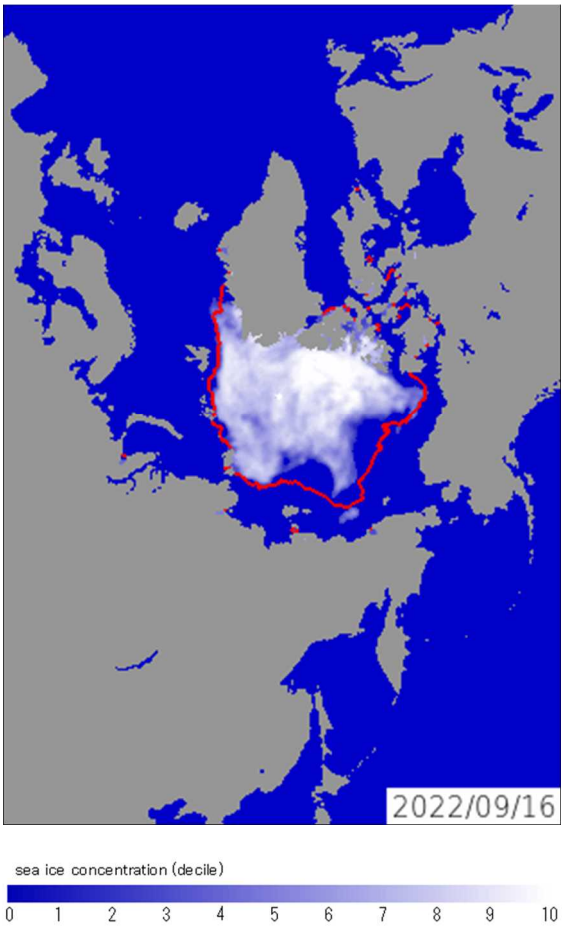

Figure 5-3 Annual minimum Arctic sea ice distribution
As of 16 September 2022. Red lines represent the normal extent. The base period for the normal is 1991 – 2020.

(ADACHI Noriyuki, Office of Marine Prediction)

<<Table of contents <Top of this article

TCC and WMC Tokyo co-contributions to Regional Climate Outlook Forums

WMO Regional Climate Outlook Forums (RCOFs) bring together national, regional and international climate experts on an operational basis to produce regional climate outlooks based on input from participating NMHSs, regional institutions, Regional Climate Centres (RCCs) and global producers of climate predictions. By providing a platform for countries with similar climatological characteristics to discuss related matters, these forums ensure consistency in terms of access to and interpretation of climate information.

In spring 2022, experts from TCC and the World Meteorological Centre (WMC) Tokyo gave presentations on climate outlooks and TCC activities at the following RCOFs, which were held online due to the ongoing COVID-19 pandemic.

- the 18th session of the Forum on Regional Climate Monitoring, Assessment and Prediction for Regional Association II (FOCRA II-18)
- the 22th summer session of the South Asian Climate Outlook Forum (SASCOF-22)

As part of collaborative activities between TCC and WMC Tokyo, the experts from TCC and WMC Tokyo provided summer season outlooks including probabilistic forecasts based on JMA's dynamical seasonal ensemble prediction system as well as Copernicus Climate Change Service (C3S) multi-model ensemble prediction, which the Japan Meteorological Agency (JMA) has joined in since October 2020. The presenters also covered climate monitoring and highlighted efforts to promote the use of TCC climate prediction information. These activities are intended to support the output of country-scale outlooks by National Meteorological and Hydrological Services (NMHSs), contribute to the summarization of consensus outlooks and reduce climate disaster risks in the water, agriculture and health sectors for each target area. TCC and WMC Tokyo are committed to collaboration with operational climate communities to enhance progress in forecast skill and application of climate information toward the resolution of common issues and realizing a climate-resilient world.

(NEMOTO Noboru, TAKAHASHI Kiyotoshi, Tokyo Climate Center)

<<Table of contents <Top of this article

TCC contributions to the Report on the States of the Climate in Asia 2021

WMO's State of the Climate in Asia 2021 report was published 14th November 2022 as the second in the series, summarizing climatic conditions and extreme weather events observed in 2021 and associated socioeconomic impacts in the Asian region (RA II). The report is intended for widespread reference in various fields relating to climate change.

The contributions of National Meteorological and Hydrological Services (NMHSs) and WMO Regional Climate Centers (RCCs) in the region were essential In compiling this report. TCC again made a significant contribution with its drafting of input on Extreme Events and Tropical Cyclones and other areas. Ongoing collaboration among Members and RCCs in RA II will support future reporting in this field for the Asian region.

URL: https://library.wmo.int/index.php?lvl=notice_display&id=22158#.Y4IjI3bP1D9

(NEMOTO Noboru, TAKAHASHI Kiyotoshi, Tokyo Climate Center)

<<Table of contents <Top of this article

You can find the latest newsletter from the Japan International Cooperation Agency (JICA).

JICA Magazine

https://jicamagazine.jica.go.jp/en/

"JICA magazine" is a public relations magazine published by JICA. It introduces the current situations of developing countries around the world, the people who are active in the field, and the content of their activities.

Any comments or inquiry on this newsletter and/or the TCC website would be much appreciated.
Please e-mail to tcc@met.kishou.go.jp.
(Editors: NEMOTO Noboru, TAKAHASHI Kiyotoshi)

Tokyo Climate Center, Japan Meteorological Agency
3-6-9 Toranomon, Minato City, Tokyo 105-8431, Japan

TCC Website:
https://www.data.jma.go.jp/tcc/tcc/index.html

<<Table of contents